LRP 621/98 October 1998

Stability Analysis of the Vertical Position Control Loop in TCV Using Rigid and Deformable Plasma Models

F. Hofmann, J.-M. Moret, D.J. Ward

Accepted for publication
in
NUCLEAR FUSION

Stability Analysis of the Vertical Position Control Loop in TCV Using Rigid and Deformable Plasma Models

F. Hofmann, J.-M. Moret, D.J. Ward*

Centre de Recherches en Physique des Plasmas,

Association EURATOM - Confédération Suisse,

Ecole Polytechnique Fédérale de Lausanne, CH-1015 Lausanne, Switzerland

Abstract:

The stability of the vertical position control system in TCV is analyzed using two different plasma models, a deformable plasma model (DPM) and a rigid plasma model (RPM). Open loop growth rates and closed loop stability are computed, as a function of various plasma parameters for both models. It is found that the difference between the open loop growth rates predicted by the two models depends significantly on plasma elongation and triangularity. Growth rates are also computed using the NOVA-W code and good agreement is found with the DPM results. The stability of the closed loop system is analyzed as a function of the feedback gain settings. The size of the stable domain in gain space is evaluated for the DPM and RPM models as a function of plasma elongation and triangularity, and the effect of varying the vertical position observer is shown. The stable domains, as predicted by the two models, are consistent with experimental observations obtained from a highly elongated, D-shaped plasma in TCV (κ=2.55).

*present address: Lawrence Livermore National Laboratory, Livermore, CA 94551, U.S.A.

1. Introduction

The benefits of elongated and shaped plasma cross-sections, i.e., higher beta limits and better confinement, are by now generally acknowledged, and practically all new tokamak designs use these concepts. However, elongated cross-sections inevitably lead to vertically unstable plasmas, requiring a passive shell and active feedback coils for stabilization. The vertical position feedback loop in an elongated tokamak is a highly complex system consisting of vertical position detectors, signal processors, power supplies, active coils, passive stabilizers, and the plasma itself. The stability of this system depends on a very large number of parameters and the only practical way to optimize these parameters is to construct a sufficiently accurate model and to analyze the stability of the model. Modelling tokamak hardware is a fairly straightforward enterprise, but modelling the plasma is not trivial. A large number of plasma models have been used in the past.

Perhaps the simplest of all models is a single current-carrying filament [1-3]. This model can be used for rough scoping studies but it is known to be inaccurate for highly elongated and D-shaped plasmas. A slightly more sophisticated approach consists of assuming that the plasma behaves as if it were a rigid body and that its motion is constrained to strictly vertical displacements. Several varieties of this model have been proposed [4-10]. Some of these assume that the poloidal flux at the plasma surface is fixed during the vertical motion. This will, in general, lead to a surface current [11]. Rigid plasma models have been shown to predict open loop growth rates fairly accurately [12] but there are experimental situations where plasma deformation cannot be neglected [13,14]. In addition, it is not clear whether the rigid plasma model is suitable for closed loop stability analysis, especially when one is considering highly elongated plasmas [14]. The open loop growth rate is defined here as the linear growth rate of the most unstable axisymmetric mode, taking into account induced toroidal currents in the passive shell but neglecting variations of the poloidal field coil currents. Closed loop stability, on the other hand, refers to the stability of the complete vertical position control loop as a function of the gain settings used in the controller.

Going one step further in complexity, we find the perturbed equilibrium models [15-18]. These models include the effects of plasma deformation but, in some cases, they violate ideal MHD constraints. Results obtained from such models have been compared to experiments [17,19,20] and good agreement is obtained for moderately elongated plasmas with low open loop growth rates. However, it remains to be seen whether these models are still valid for highly elongated plasmas with high growth rates and low stability margins. Ideal MHD codes have also been used to investigate the problem of axisymmetric stability [21-25] but these codes are usually expensive in terms of computer time and cannot easily be used for system optimization in multi-dimensional parameter space.

In this paper, we propose a deformable plasma model (DPM), based on calculations of poloidal flux perturbations, produced by current perturbations in the active feedback coils and passive structures. Although this model belongs to the family of perturbed equilibrium models, it is actually equivalent to more elaborate ideal MHD models, such as NOVA-W [24], if we consider axisymmetric modes only and if plasma inertia can be neglected. The model is described in detail in section 2. In section 3, we compare open loop growth rates obtained with the deformable plasma model with those obtained from a rigid plasma model (RPM). In section 4, we analyze the closed loop stability of the TCV vertical position control system and we show the influence of the plasma model. Section 5 deals with the effect of the vertical position observer on the discrepancy between the two models, and section 6 compares the predicted closed loop stability limits with experimental observations in TCV.

2. Plasma Models

2.1. Deformable Plasma

If we neglect plasma inertia, the problem of axisymmetric stability can be treated on the basis of a plasma model consisting of a number of perturbed equilibria, produced by perturbed currents in the active coils and passive structures. Plasma inertia can indeed be neglected, in the present study, since the plasma motion is several orders of magnitude

slower than the Alfvén time scale. Let us consider a free-boundary tokamak equilibrium, as represented by a solution of the Grad-Shafranov equation,

$$(1/R)\,(\partial^2\Psi/\partial Z^2) + (\partial/\partial R)\,[(1/R)\,(\partial\Psi/\partial R)] = -\mu_0 R\, p'(\Psi) - (1/R)\, ff'(\Psi) \qquad (1)$$

where Ψ is the poloidal flux, p' and ff' are the usual source functions and the prime indicates differentiation with respect to Ψ. The solution of (1) is obtained either from a reconstruction of an experimental equilibrium [26] or from a straightforward free-boundary equilibrium calculation [27]. We now introduce a perturbation in one or several of the external currents. This will give rise to a perturbed equilibrium with a perturbed poloidal flux, $\Psi_1=\Psi+\delta\Psi$, and perturbed source functions, $(p')_1=p'+\delta(p')$, $(ff')_1=ff'+\delta(ff')$. The perturbations must satisfy the equation

$$(1/R)\,(\partial^2\delta\Psi/\partial Z^2) + (\partial/\partial R)\,[(1/R)\,(\partial\delta\Psi/\partial R)] =$$
$$-\mu_0 R\,[p''(\Psi)\delta\Psi + \delta p'(\Psi)] - (1/R)\,[(ff')'(\Psi)\delta\Psi + \delta(ff')(\Psi)] \qquad (2)$$

where all second order terms have been dropped. Eq.(2) can be solved by an iterative method similar to the one which is used in free-boundary equilibrium calculations [27]. The functions, $\delta(p')$ and $\delta(ff')$, are recomputed at each iteration by imposing the ideal MHD constraints of flux conservation, $\delta q=0$, and adiabaticity, $(\delta p/p)= -(5/3)(\delta V'/V')$. Here, q is the safety factor and $V(\Psi)$ is the volume enclosed by the flux surface with label Ψ. It is clear that, in order to construct a complete plasma model, we have to compute perturbed equilibria for all conceivable coil current and vessel current perturbations. An arbitrary perturbed equilibrium can then be obtained from a linear superposition of the perturbations due to individual currents.

In this paper, our aim is to analyze the stability of the vertical position control system in TCV. For this purpose, it is sufficient to consider up-down symmetric configurations with up-down antisymmetric perturbations. More precisely, we assume that the plasma, the poloidal field coils, the active feedback coils and the passive structures are all symmetric with

respect to the equatorial plane, Z=0. In addition, since we are interested in vertical plasma motion, we consider up-down antisymmetric perturbations, creating radial magnetic fields. This implies that any perturbed current in the upper half plane, Z>0, has its mirror image in the lower half plane, Z<0, with inverted perturbation. In this case [25], both the poloidal flux and the toroidal plasma current density, j, which is proportional to the r.h.s. of eq.(1), must remain unperturbed on the equatorial plane,

$$\delta\Psi = 0, \text{ for } Z=0 \tag{3}$$

and

$$- \mu_0 R[\delta(p')(\Psi)] - (1/R)[\delta(ff')(\Psi)] = 0, \text{ for } Z=0 \tag{4}$$

Eq.(4) can be satisfied for an arbitrary value of the major radius, R, only if the two functions, $\delta(p')(\Psi)$ and $\delta(ff')(\Psi)$ are identically zero. In other words, the source functions remain unchanged by an antisymmetric perturbation of an up-down symmetric equilibrium.

As an example, let us consider a highly elongated, D-shaped equilibrium with κ=2.75 and δ=0.49, generated by the FBT code [27]. We perturb this equilibrium by up-down antisymmetric currents in the vacuum vessel. For this purpose, we decompose the vacuum vessel into 38 ring-shaped elements (Fig. 1). Each element is characterized by a resistance and a self-inductance. Resistances are measured by inducing localized toroidal currents in the vacuum vessel, using the poloidal field coils. Inductances are calculated, based on the known geometry of the vessel. The first and the 20th elements lie on the equatorial plane and hence, the currents in these elements always remain zero. The remaining 36 elements can be combined into 18 pairs of elements such that each pair consists of one element in the upper half plane and its mirror image in the lower half plane. The currents in the two elements of a pair are always equal and opposite. Fig. 2 shows contour plots of the plasma current perturbation as a result of a current perturbation in some of the 18 pairs of vessel elements. Similar contour plots of the perturbed poloidal flux are shown in Fig. 3.

2.2. Rigid Plasma

If the plasma is considered to be a rigid body, the perturbed plasma current density resulting from a vertical displacement, δZ, is simply given by

$$\delta j = (\partial j/\partial Z)\, \delta Z \tag{5}$$

where j is the toroidal current density of the unperturbed equilibrium. The requirement that all vertical forces acting on the displaced plasma must add up to zero is then expressed as

$$\int (\delta j\, B_r + j\, \delta B_r)\, dV = 0 \tag{6}$$

where B_r is the radial magnetic field produced by the external coil currents of the unperturbed equilibrium and δB_r is produced by the perturbation of the external currents. In this model, the plasma current perturbation is independent of the type of excitation. An example, based on the same unperturbed equilibrium as was used above (κ=2.75 and δ=0.49) is shown in Fig. 4.

3. Open Loop Growth Rates

The axisymmetric evolution of a vertically unstable plasma within a resistive shell can be described by an eigenvalue equation,

$$R_v\, \mathbf{I}_v + \gamma\, (L_{vv} + T_{vv})\, \mathbf{I}_v = 0 \tag{7}$$

where $\mathbf{I}_v$ is a suitably normalized distribution of currents in the vessel elements, R_v and L_{vv} are the resistance and inductance matrices, γ is the growth rate and the term $\gamma T_{vv}\, \mathbf{I}_v$ gives the voltages induced by the plasma response to perturbed vessel currents. The matrix T_{vv} depends on the plasma model, and for the two models presented above, it can be readily computed.

In order to show the influence of the plasma model, we compute open loop growth rates as a function of elongation and triangularity. We consider up-down symmetric plasmas within the TCV vacuum vessel (Fig. 1) and we neglect induced currents in the poloidal field coils. Fig. 5 shows the results of κ-scans for two different values of δ and Fig.6 shows δ-scans for three values of κ. In all these scans, the safety factor at the 95% flux surface, q_{95}, was kept constant, q_{95} =2.90. We note that, at low elongation and low triangualrity, the two models give the same growth rate. As the triangularity increases, the DPM becomes more unstable than the RPM, but increasing the elongation has the opposite effect. If we increase both κ and δ, the two effects cancel and we can find cases (e.g. κ=2.4, δ=0.46) where the two models again predict the same growth rate.

A tentative explanation of these rather unexpected results can be obtained by considering the structure of the unstable modes. If we decompose the plasma displacement into poloidal harmonics, we find that the RPM only takes the m=1 component into account, whereas the DPM, just as NOVA-W, includes many poloidal harmonics. It is known that the m=2 and m=3 components are very important at high elongation and triangularity [25]. The effect of these higher harmonics on the growth rate of the eigenmode can be either positive or negative, depending on the shape of the plasma boundary and the shape of the conducting shell. In the case of TCV, the plasma shape can be described approximately by

$$R = R_0 + a[\cos(\theta+\delta \sin\theta - \lambda \sin 2\theta)], \quad Z = Z_0 + a\,\kappa \sin\theta \qquad (8)$$

where R_0 and a are the major and minor radii, respectively, Z_0 measures the vertical position of the magnetic axis and λ is the rectangularity. Since the TCV vacuum vessel has a rectangular shape, we usually take $\lambda>0$ at high elongation in order to improve vertical stability. In the present study, we assume that λ increases with κ, $\lambda=(\kappa-1.07)/6.67$. Under these conditions, the higher poloidal harmonics apparently have a stabilizing effect when the elongation increases and a destabilizing effect when the triangularity increases.

The open loop growth rate not only depends on the plasma shape but also on the plasma current distribution. This can be seen in Fig. 7, where we plot RPM and DPM

growth rates as a function of the internal inductance, l_i, for a fixed plasma shape (κ=1.8, δ=0.5). It is seen that, as l_i increases, the results of the two models converge. This is consistent with the results shown in Fig. 6 if one considers that vertical stability depends on "effective" shape parameters which are somehow averaged over the plasma cross-section. For high values of l_i, the plasma current distribution is peaked and the central elongation and triangularity are quite small. Consequently, the "effective" shape parameters are also small and hence, according to Fig. 6, the two models ought to give the same result.

A comparison of NOVA-W and DPM results is shown in Fig. 8. We find good agreement over a wide range of growth rates. Open loop growth rates have also been measured experimentally in TCV and a comparison between measured and calculated growth rates has shown that the NOVA-W model gives much better agreement with experimental results than the rigid current model [12].

4. Closed Loop Stability

The stability of the vertical position feedback loop in TCV has been studied recently using the RPM and NOVA-W models [10,25]. However, the influence of the plasma model on the results cannot be judged from these studies because the feedback strategy and the power supply models used in the two cases were completely different. In this paper, we use the assumptions of Ref. [10] as they closely match experimental conditions in TCV. The analysis presented in [10] is extended to cover the two plasma models, DPM and RPM, as discussed in section 2. Vertical position control in TCV is accomplished by slow coils outside the vacuum vessel and two fast coils inside the vessel [10]. Any combination of shaping coils can be used as slow coils. In this study, we use four outboard shaping coils (F2, F3, F6, F7) for vertical position control, in accordance with recent experiments [10]. The slow coils have a typical response time of 1ms. The two fast coils are located in the outboard corners of the vacuum vessel (Fig. 1), and their response time is approximately 0.1ms. The vertical position control loop consists of a ZI_p observer, based on magnetic measurements [28], a PD controller, slow and fast active coils with their power supplies and

the vacuum vessel which serves as a passive stabilizer. The complete system can be described by the five equations

$$\mathbf{V}(t) = R\,\mathbf{I} + (L + T)\,\partial\mathbf{I}/\partial t \tag{9}$$

$$V_S(t+\Delta) = P[\Omega_1 \cdot \Psi + \Omega_2 \cdot \mathbf{B}] + D[\Omega_3 \cdot \partial\Psi/\partial t + \Omega_4 \cdot \partial\mathbf{B}/\partial t] \tag{10}$$

$$V_F(t+\delta) = G[\Omega_5 \cdot \partial\mathbf{B}/\partial t] \tag{11}$$

$$\Psi = (W_1 + H_1)\,\mathbf{I} \tag{12}$$

$$\mathbf{B} = (W_2 + H_2)\,\mathbf{I} \tag{13}$$

where **V** and **I** are vectors containing the voltages and currents of all active feedback coils and vessel elements. R and L are the resistance and inductance matrices, respectively, and the term T ($\partial\mathbf{I}/\partial t$) gives the voltages which are induced by the plasma response to currents in the active coils and vessel elements. $V_S(t+\Delta)$ and $V_F(t+\delta)$ are the voltages applied to the slow and fast coil, respectively. These signals are delayed, by the time intervals Δ and δ, with respect to the signals obtained from the vertical position observers, $V_S(t)$ and $V_F(t)$. Typical values of these delays in TCV are Δ=1.0ms and δ=0.2ms. P, D and G are the feedback gains and the vectors Ω_1, Ω_2, Ω_3, Ω_4 and Ω_5 define the vertical position observer. Ψ and **B** are the poloidal fluxes and magnetic fields at the positions of the flux loops and magnetic field probes (Fig. 1). The matrices W_1 and W_2 contain Green's functions describing the fluxes and magnetic fields which are produced directly by coil currents and vessel currents, whereas the matrices H_1 and H_2 describe the fluxes and fields produced by the plasma response to coil currents and vessel currents. The matrices T, H_1 and H_2 are computed from the perturbed plasma current densities, which depend on the plasma model assumed, as described in section 2.

The model of the vertical position control loop, as given by Eqns. (9) - (13), is complete in the sense that it describes all the elements of the real experiment without major simplifying assumptions. The accuracy of the model depends mainly on the accuracy of the various coefficients used in the equations. We have tried to evaluate these coefficients as precisely as possible, but there are still a few areas where the model could be improved. For example, voltage and current saturation in the power supplies is not included in the present model. Also, the simple delays assumed here between the observer output and the coil voltages do not describe the real transfer functions correctly over the entire frequency range. Inspite of these shortcomings, we believe that the model is sufficiently accurate for the purpose of the present study, i.e., for showing the effect of the plasma model on open loop and closed loop stability predictions.

Analyzing the system of equations (9) - (13), we find that, for any given combination of the feedback gains, P, D and G, there are either growing exponential solutions or growing oscillatory solutions or no growing solutions at all. If we assume a fixed fast gain G, we can divide the P-D plane into stable and unstable domains [10]. On the boundary between stable and unstable domains, the growth rate of the closed loop system is zero, but the oscillation frequency remains finite. In Fig. 9, we show the stable domains in the P-D plane, as a function of elongation, for D-shaped plasmas in TCV. The figure compares results obtained with the two plasma models, RPM and DPM. Here, the fast gain G was adjusted at each elongation such that the size of the stable domain, using the DPM, remained approximately constant. At each elongation, the fast gain used with the RPM was the same as that used with the DPM. Fig. 9 shows that the RPM predicts a much larger the stable domain in gain space than the DPM, especially at high elongation, inspite of the fact that RPM and DPM open loop growth rates are quite similar for these plasmas (Fig. 5). This surprising result is clear evidence for the fact that the mode structure in the closed loop case is completely different from the mode structure in the open loop case [25]. It should be noted that, in Fig. 9, the fast gain, G, increases with elongation in order to maintain the size of the stable domain of the DPM. As a result, the stable domain of the RPM grows with elongation which, of course, does not imply that the plasma becomes inherently more stable with increasing elongation.

Closed loop stability also depends on triangularity, as shown in Fig. 10. Here, the divergence between the two models increases with increasing triangularity in a similar fashion as was observed for the open loop growth rate at low elongation (Fig.6).

5. Effect of the Vertical Position Observer

The observers that have been used in the stability analyses presented above are all taken from actual TCV discharges [10]. They are highly optimized, using the methods presented in [29]. A typical example is shown in Fig. 11a, where we plot the coefficients which multiply the signals obtained from the B-probes, Ω_5, as a function of probe number. The other components of the vertical position observer (Eqns. 10 and 11) are assumed as $\Omega_2=\Omega_4=\Omega_5$ and $\Omega_3=\Omega_1$ where Ω_1 is given in Ref. [10]. It is known that non-optimized observers can severely limit the performance of the feedback system [25]. Let us consider two examples of non-optimized observers. The first (Fig. 11b) consists of a single pair of flux loops and B-probes, located on the inboard wall of the vacuum vessel (#6 and #34 in Fig. 1). To test this observer, we consider a highly elongated, D-shaped plasma (κ=2.75 and δ=0.49), and we adjust the fast gain G such that there is a small stable island in P-D space, using the DPM. For the same fast gain, the RPM then predicts a very large stable domain, as shown in Fig. 12. The second non-optimized observer we wish to consider (Fig. 11c) is a pair of flux loops and B-probes, located on the outboard wall of the vessel (#18 and #22 in Fig. 1). Here, we find that the RPM still predicts a stable domain, whereas the DPM gives unstable solutions throughout the P-D plane (Fig.12). We conclude from these results that, while it is generally important to take the effects of plasma deformation into account in computing closed loop stability, especially at high κ and δ, it becomes absolutely necessary to include these effects if one considers observers based on few localized measurements.

6. Comparison with Experiments in TCV

Predictions of closed loop stability in TCV, based on the RPM, have recently been compared with experimental results, and fairly good agreement was found [10]. However, these comparisons were limited to elongations below 1.95 and low triangularities. Under

these conditions, the two plasma models, RPM and DPM, give rather similar results. In this paper, we wish to compare the model predictions with experiments at high elongation and high triangularity, where the difference between the two models is most pronounced. Let us consider a recent TCV discharge, #13049, where a highly elongated, D-shaped plasma was created with κ=2.55, δ=0.37. The free-boundary equilibrium of this discharge was reconstructed with the LIUQE code [26], using the experimental measurements, and the stability of the vertical position control loop was calculated by solving eqns. (9) - (13). The stable domain, as predicted by the two models is shown in Fig. 13. The experimental values of P and D are also shown in the figure. Since the experimental point falls within the stable domain of both models, a definite conclusion about the relative accuracy of the models cannot be drawn from this comparison. However, we believe that the DPM prediction is closer to reality since in these experiments, the stable window for D was extremely small, typically $\pm$ 5%.

7. Conclusions

Open loop growth rates and closed loop stability of the TCV vertical position control system have been computed using two different plasma models. The first model (DPM) is a deformable plasma model, based on calculations of the perturbed poloidal flux due to perturbed currents in the active feedback coils and the vacuum vessel. This model is more general than previous models of this kind in that it satisfies ideal MHD constraints and can compute perturbed source functions self-consistently. The second model (RPM) considers the plasma to be a rigid body, with a fixed current density distribution, whose motion is constrained to vertical displacements. The models have been applied to up-down symmetric configurations with up-down antisymmetric perturbations. The comparison of open loop growth rates shows that the results of the two models agree at low κ and low δ (κ=1.4, δ=0) and that the ratio between the DPM and RPM growth rates increases with δ but decreases with κ. The open loop growth rate also depends on the plasma internal inductance, l_i, and at high values of l_i, the two models give the same result.

Closed loop stability has been computed, as a function of elongation and triangualrity. We find areas in parameter space (high κ, high δ) where the open loop growth rates of the models agree fairly well, but the predictions of closed loop stability are vastly different. In other areas (moderate κ, low δ) there is considerable disagreement between the open loop growth rates and yet, the closed loop stable domains are similar in size. This behaviour is attributed to the structure of the eigenmode which has been shown to be completely different in the open loop and closed loop cases [25]. The discrepancy between the two models not only depends on the plasma parameters, but also on the choice of the vertical position observer. Examples show that this discrepancy can be very large indeed if one considers observers consisting of single pairs of flux loops and B-probes. The comparison of closed loop stability predictions with experimental results in TCV shows that both the RPM and the DPM models are consistent with the experiment, although the predicted stable domains of the two models are quite different. Additional experiments, in particular systematic scans of the feedback gains, will be necessary to decide which of the two models gives better agreement with the measurements. However, if we consider the fact that measured open loop growth rates agree much better with NOVA-W results than with RPM results [12], and if we assume the NOVA-W and DPM models to be equivalent (Fig. 8), we are led to the conclusion that the DPM model is considerably more accurate than the RPM model.

Acknowledgements

This work was partly supported by the Fonds National Suisse de la Recherche Scientifique.

References

[1] Jardin, S.C., Larrabee, D.A., Nucl. Fusion **22** (1982) 1095.

[2] Mori, M., Suzuki, N., Shoji, T. et al., Nucl. Fusion **27** (1987) 725.

[3] Lazarus, E.A., Lister, J.B., Neilson, G.H., Nucl. Fusion **30** (1990) 111.

[4] Lackner, K., McMahon, A.B., Nucl. Fusion **14** (1974) 575.

[5] Okabayashi, M., Sheffield, G., Nucl. Fusion **14** (1974) 263.

[6] Haas, F.A., Nucl. Fusion **15** (1975) 407.

[7] Rebhan, E., Nucl. Fusion **15** (1975) 277.

[8] Bobbio, S., Coccorese, E., Fabricatore, G. et al., in Controlled Fusion and Plasma Physics (Proc. 11th Eur. Conf., Aachen, 1983), Vol. 7D, Part II, European Physical Society, Geneva (1983) 539.

[9] Lister, J.B., Martin, Y., Moret, J.-M., Nucl. Fusion **36** (1996) 1547.

[10] Hofmann, F., Dutch, M.J., Favre, A. et al., Nucl. Fusion **38** (1998) 399.

[11] Hutchinson, I.H., Nucl. Fusion **29** (1989) 2107.

[12] Hofmann, F., Dutch, M.J., Ward, D.J. et al., Nucl. Fusion **37** (1997) 681.

[13] Jardin, S.C., Delucia, J., Okabayashi, M. et al., Nucl. Fusion **27** (1987) 569.

[14] Ward, D.J., Jardin, S.C., Nucl. Fusion **32** (1992) 973.

[15] Albanese, R., Coccorese, E., Rubinacci, G., Nucl. Fusion **29** (1989) 1013.

[16] Humphreys, D.A., Hutchinson, I.H., Fusion Technol. **23** (1993) 167.

[17] Tinios, G., Horne, S.F., Hutchinson, I.H. et al., Fusion Technol. **30** (1996) 201.

[18] Galkin, S.A., Ivanov, A.A., Medvedev, S.Y. et al., Nucl. Fusion **37**, (1997) 1455.

[19] Villone, F., Vyas, P., Lister, J.B. et al., Nucl. Fusion **37** (1997) 1395.

[20] Vyas, P. Villone, F. , Lister, Albanese, R., Nucl. Fusion **38** (1998) 1043.

[21] Bernard, L.C., Berger, D., Gruber, R. et al., Nucl. Fusion **18** (1978) 1331.

[22] Perrone, M.R., Wesson, J.A., Nucl. Fusion **21** (1981) 871.

[23] Lazarus, E.A., Turnbull, A.D., Kellman, A.G. et al., in Controlled Fusion and Plasma Heating (Proc. 17th European Conf., Amsterdam, 1990), Vol. 14B, Part I, European Physical Society, Geneva (1990) 427.

[24] Ward, D.J., Jardin, S.C., Cheng, C.Z., J. Comput. Phys **104** (1993) 221.

[25] Ward, D.J., Hofmann, F., Nucl. Fusion **34** (1994) 401.

[26] Hofmann, F., Tonetti, G., Nucl. Fusion **28**, (1988) 1871.

[27] Hofmann, F., Comput. Phys. Commun. **48** (1988) 207.

[28] Moret, J.-M., Bühlmann, F., Fasel, D. et al., Rev. Sci. Instrum. **69** (1998) 2333.

[29] Hofmann, F., Jardin, S.C., Nucl. Fusion **30** (1990) 2013.

Figure Captions

Fig.1 TCV poloidal cross-section, showing the OH transformer (A1, B1, B2, C1, C2, D1, D2), shaping coils (E1-E8, F1-F8), vacuum vessel, flux loops (x), magnetic field probes (–), labelled 1 to 38, and the fast coils.

Fig.2 Perturbation of the toroidal plasma current density, resulting from antisymmetric currents in two vessel elements. Current carrying elements are identified on top of each frame. Element numbers are defined in Fig. 1.

Fig.3 Perturbation of the poloidal flux produced by antisymmetric currents in two vessel elements. Current carrying elements are identified on top of each frame. Element numbers are defined in Fig. 1.

Fig.4 Perturbation of the toroidal plasma current density, resulting from a rigid vertical displacement of the entire plasma. Vacuum vessel cross-section is also shown.

Fig.5 Open loop growth rate vs. elongation for elliptical and D-shaped plasmas in TCV (q_{95}=2.90, Z_{axis}=0), obtained with DPM (solid line) and RPM (dashed line).

Fig.6 Open loop growth rate vs. triangularity for elongated plasmas in TCV (q_{95}=2.90, Z_{axis}=0) obtained with DPM (solid line) and RPM (dashed line).

Fig.7 Open loop growth rate vs. internal inductance for fixed plasma shape (κ=1.8, δ=0.5), obtained with DPM (solid line) and RPM (dashed line).

Fig.8 Comparison of open loop growth rates obtained from NOVA-W and DPM.

Fig.9 Closed loop stability in the P-D plane for three elongations and two plasma models (δ=0.49, q_{95}=2.90). Stable domain is the leaf-shaped area without symbols in the centre of each frame.

Fig.10 Closed loop stability in the P-D plane for three triangularities and two plasma models (κ=2.18, q_{95}=2.90). Stable domain is the leaf-shaped area without symbols in the centre of each frame.

Fig.11 Vertical position observer (Ω_5 in Eq.11); (a) optimized. (b) and (c) non-optimized.

Fig.12 Closed loop stability in the P-D plane for two non-optimized observers and two plasma models (κ=2.75, δ=0.49, q_{95}=2.90). Flux loops and B-probes used in the observers are identified on top of the figure. Stable domain is area without symbols.

Fig.13 Comparison of closed loop stability predictions with experimental results in TCV (κ=2.55, δ=0.37, q_{95}=2.58). Experimental P and D values are shown as open squares.

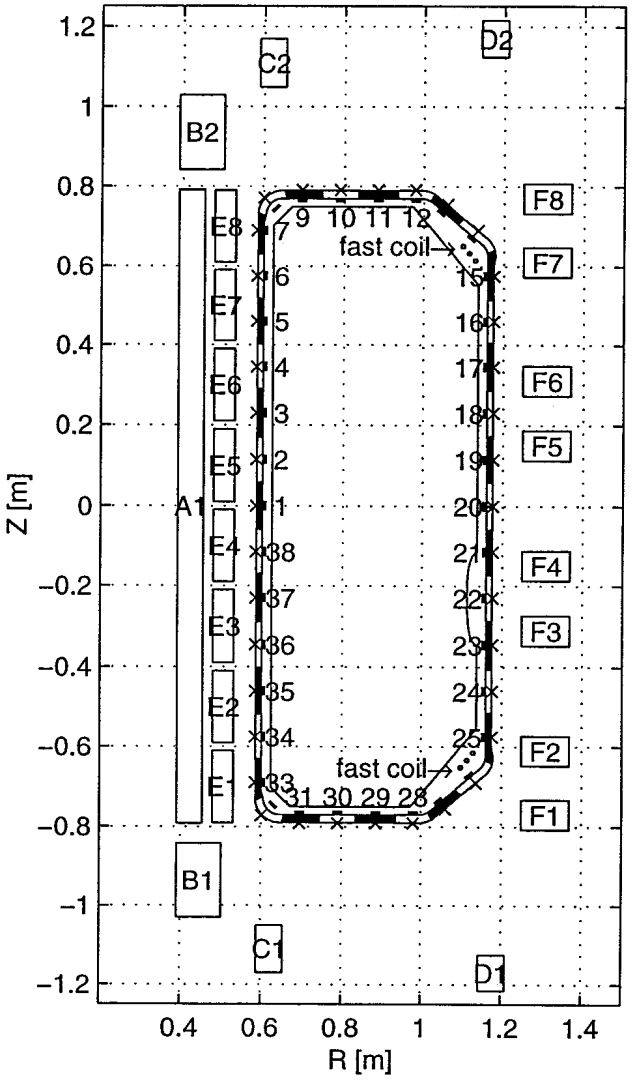
1.2
1
0.8
0.6
0.4
0.2
0
−0.2
−0.4
−0.6
−0.8
−1
−1.2
Z [m]
0.4
0.6
0.8
1
1.2
1.4
R [m]
C2
D2
B2
F8
F7
F6
F5
F4
F3
F2
F1
B1
C1
D1
A1
E8
E7
E6
E5
E4
E3
E2
E1
9 10 11 12
fast coil
7
6
5
4
3
2
1
38
37
36
35
34
33
31 30 29 28
fast coil
15
16
17
18
19
20
21
22
23
24
25

Fig.1.

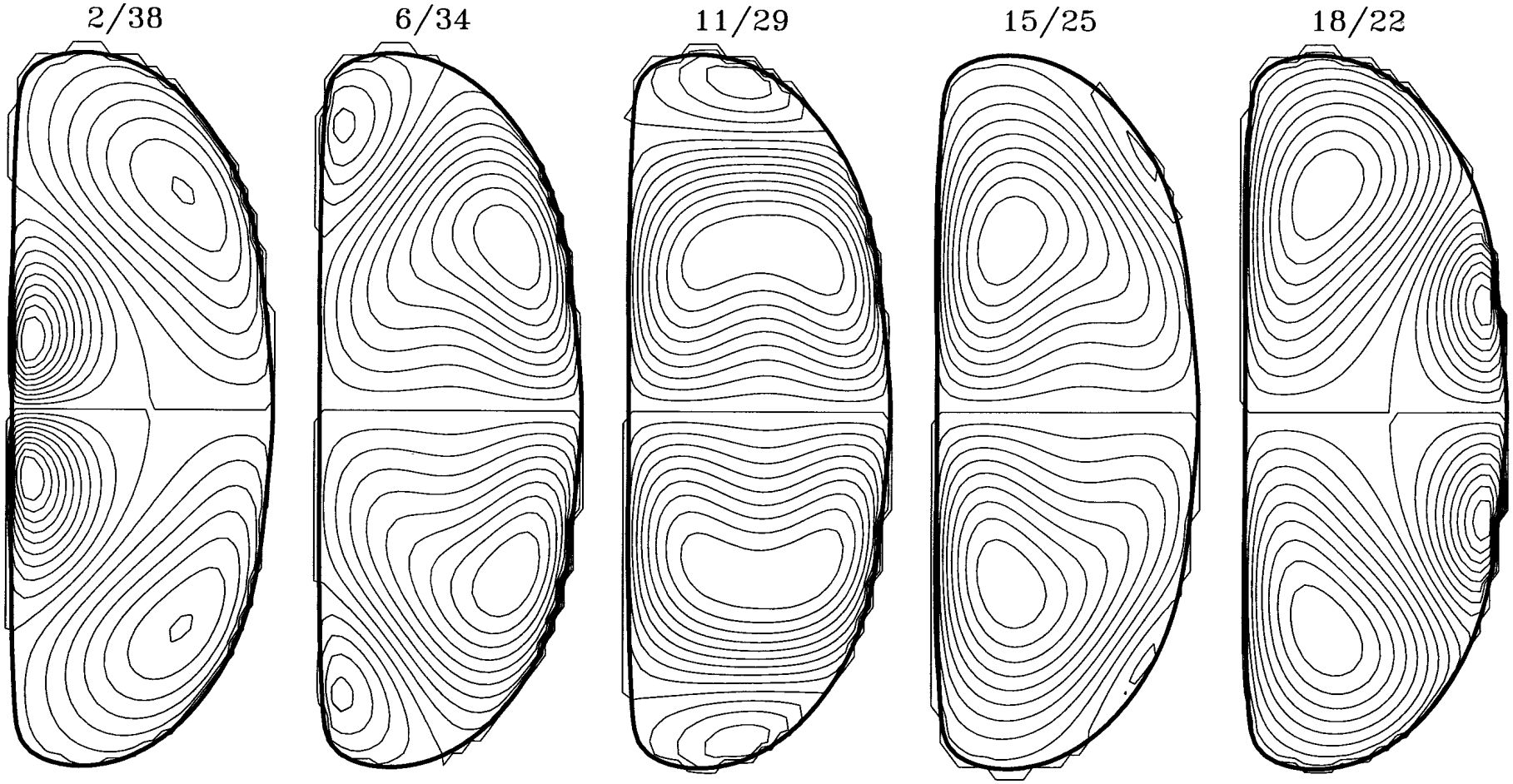

Fig.2.

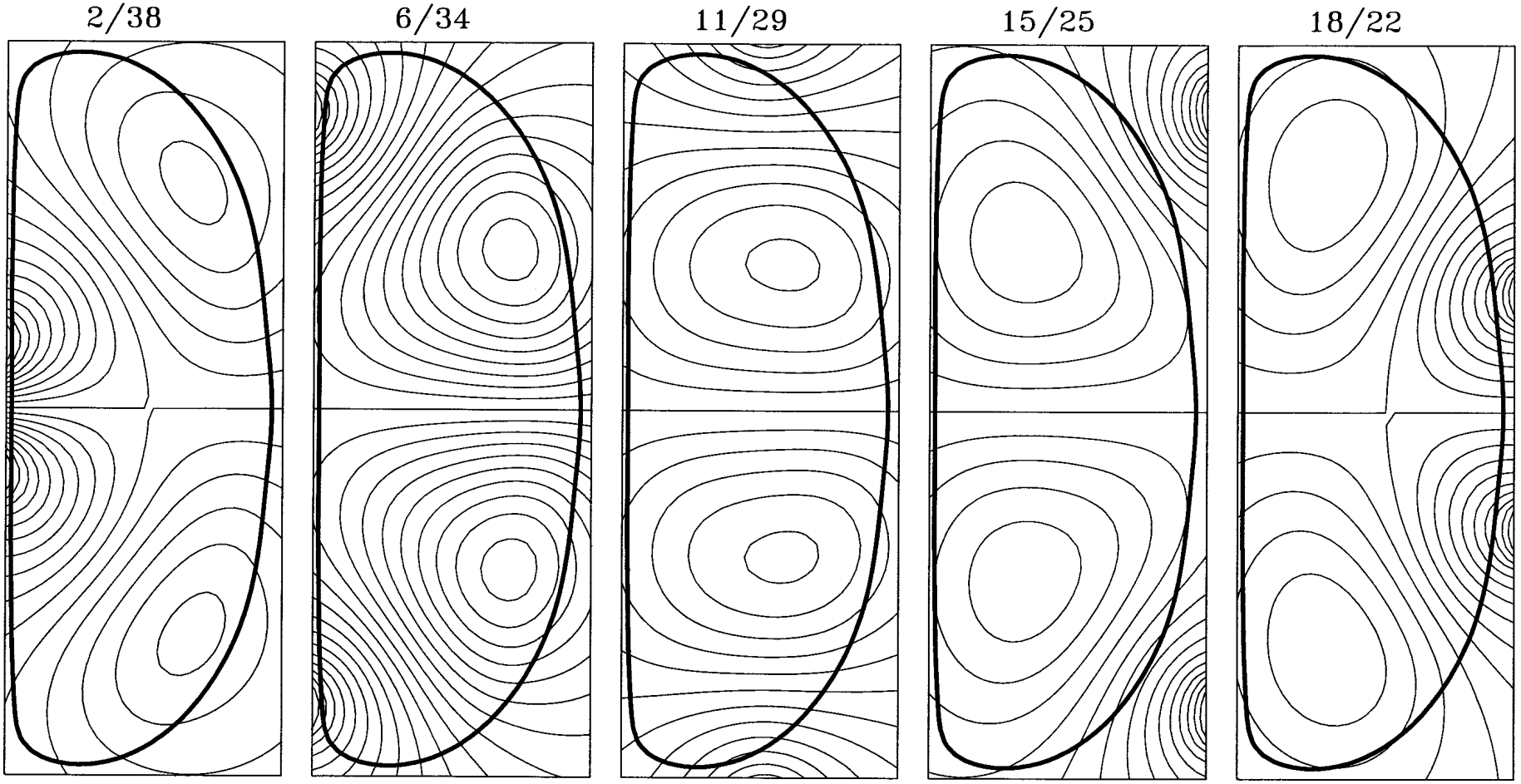

Fig.3.

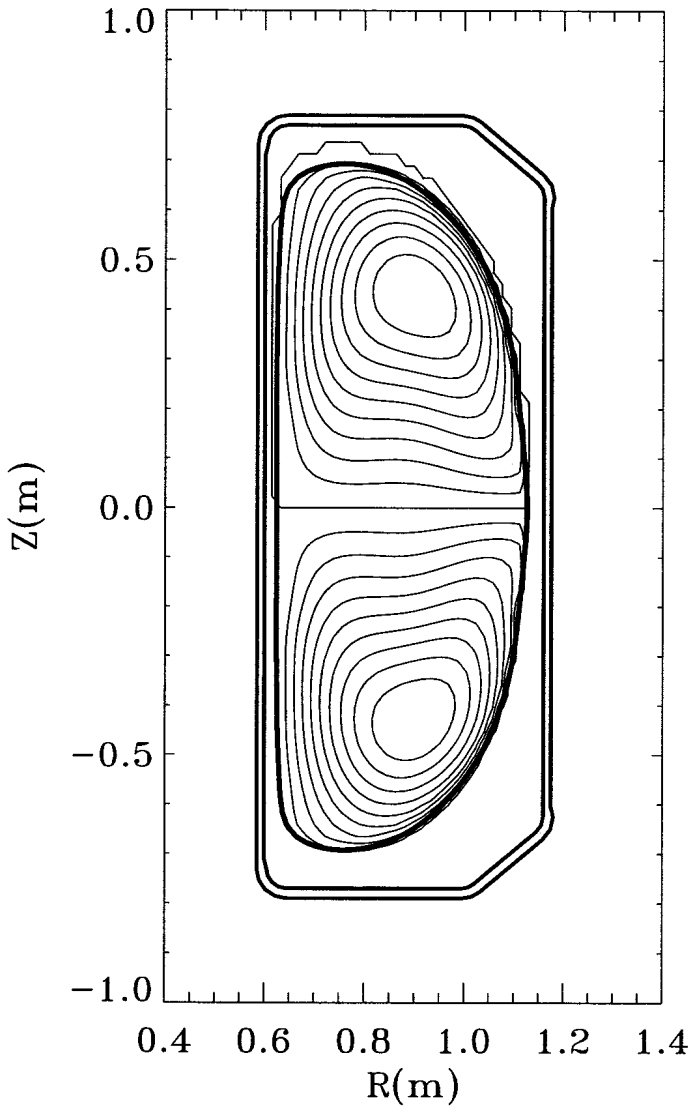

Fig.4.

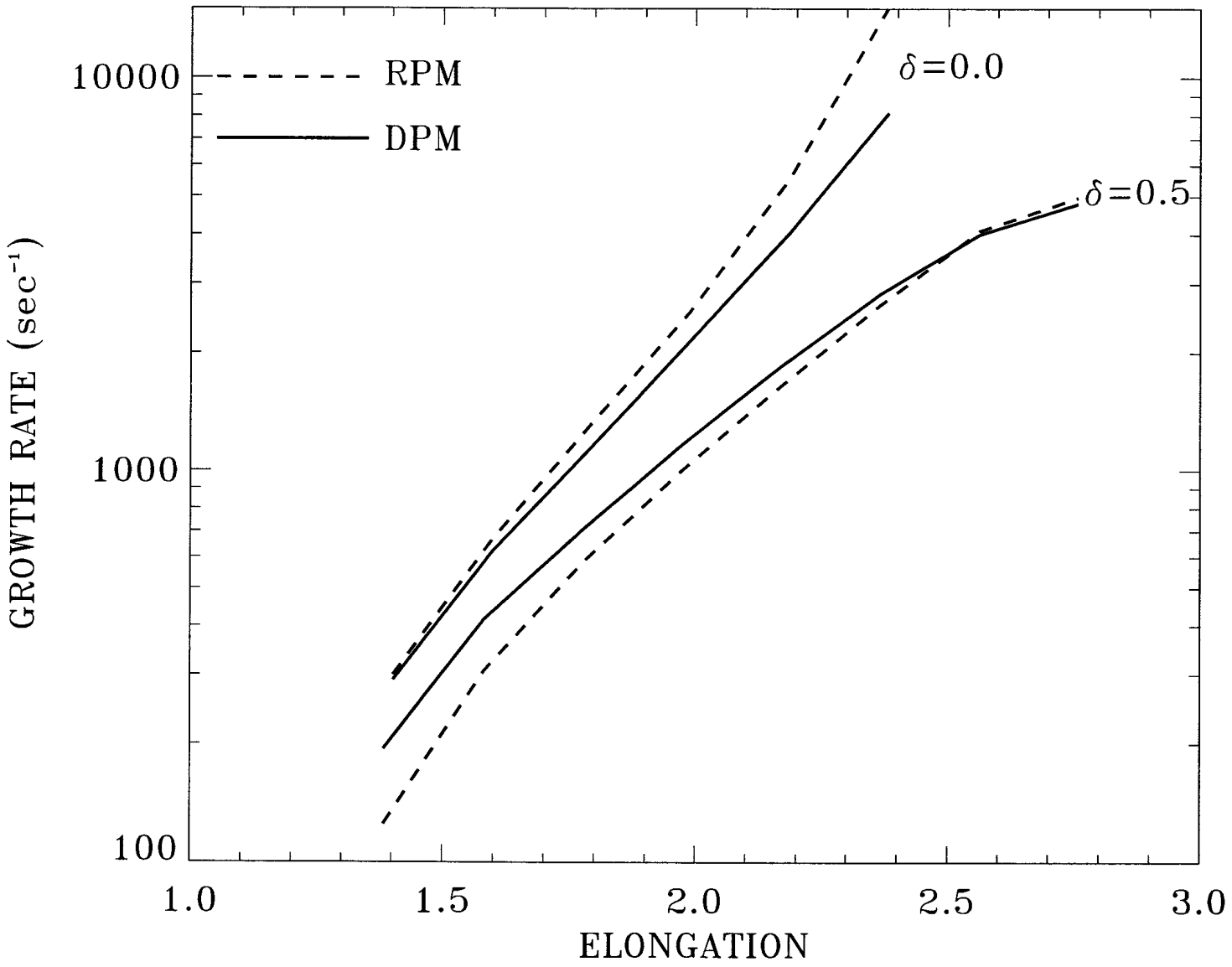
RPM
DPM
δ=0.0
δ=0.5
10000
1000
100
GROWTH RATE (sec⁻¹)
1.0
1.5
2.0
2.5
3.0
ELONGATION

Fig.5.

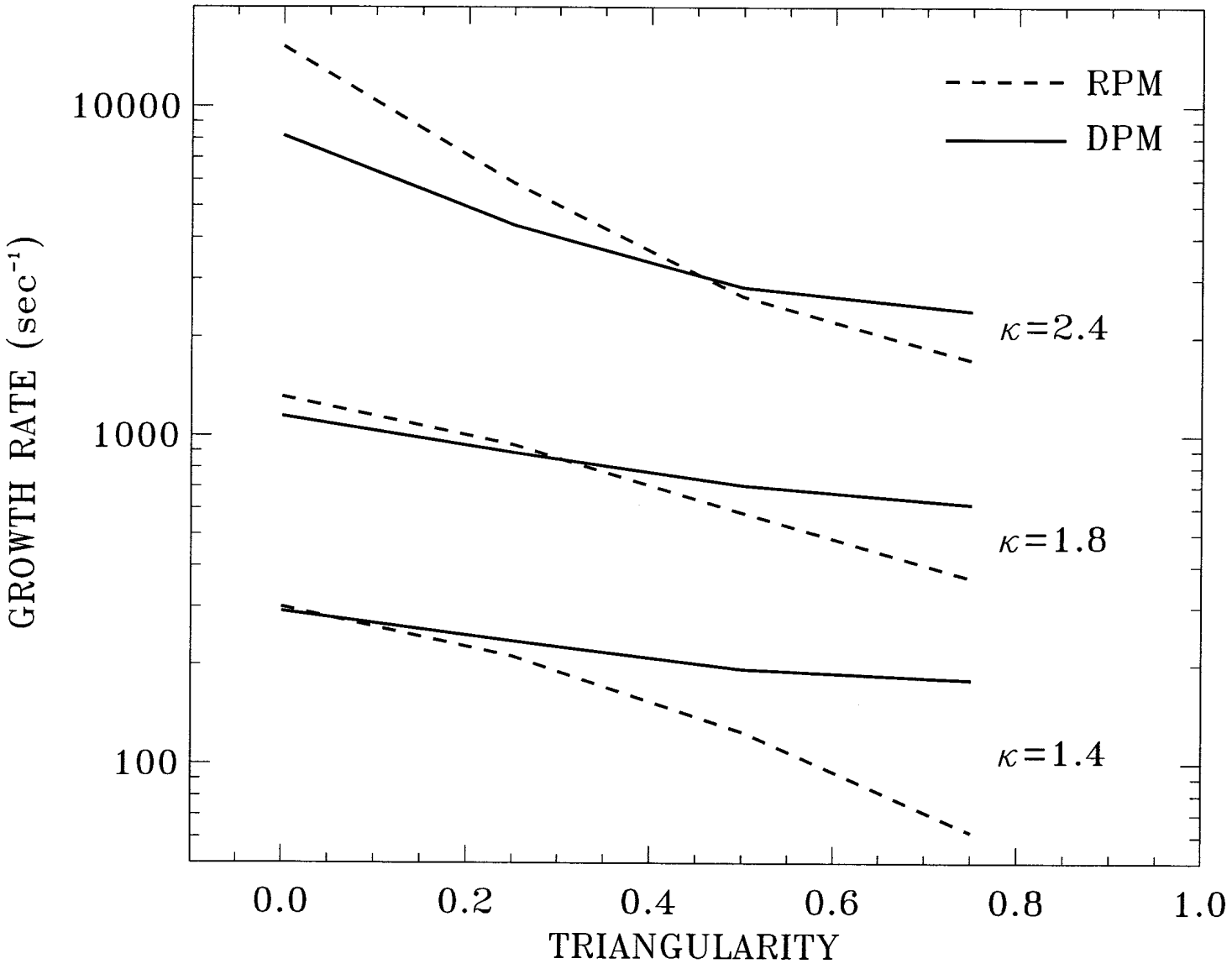
RPM
DPM
κ=2.4
κ=1.8
κ=1.4
10000
1000
100
GROWTH RATE (sec⁻¹)
0.0
0.2
0.4
0.6
0.8
1.0
TRIANGULARITY

Fig.6.

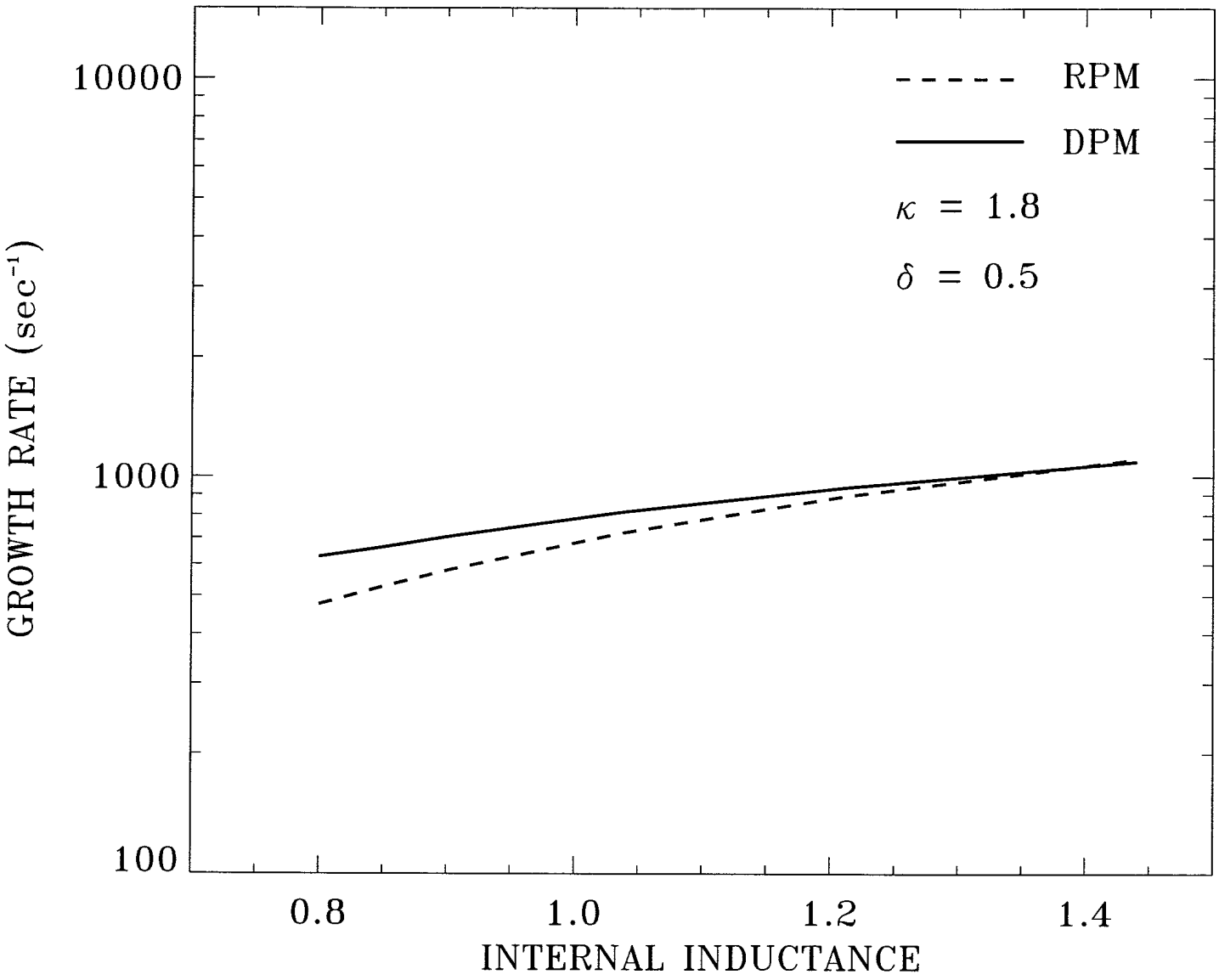
10000
1000
100
GROWTH RATE (sec^{-1})
RPM
DPM
κ = 1.8
δ = 0.5
0.8
1.0
1.2
1.4
INTERNAL INDUCTANCE

Fig.7.

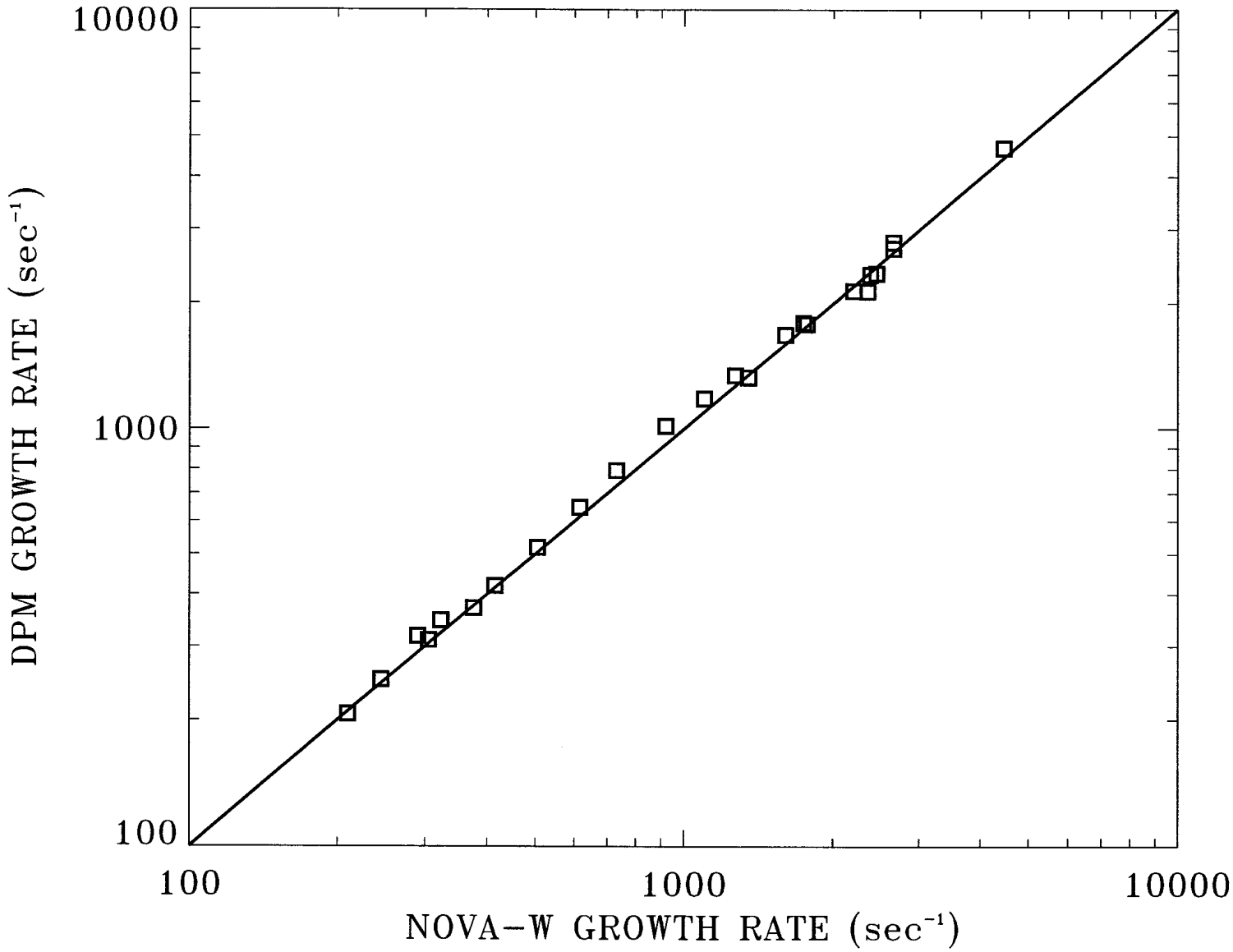
10000
1000
100
100
1000
10000
DPM GROWTH RATE (sec^{-1})
NOVA-W GROWTH RATE (sec^{-1})

Fig.8.

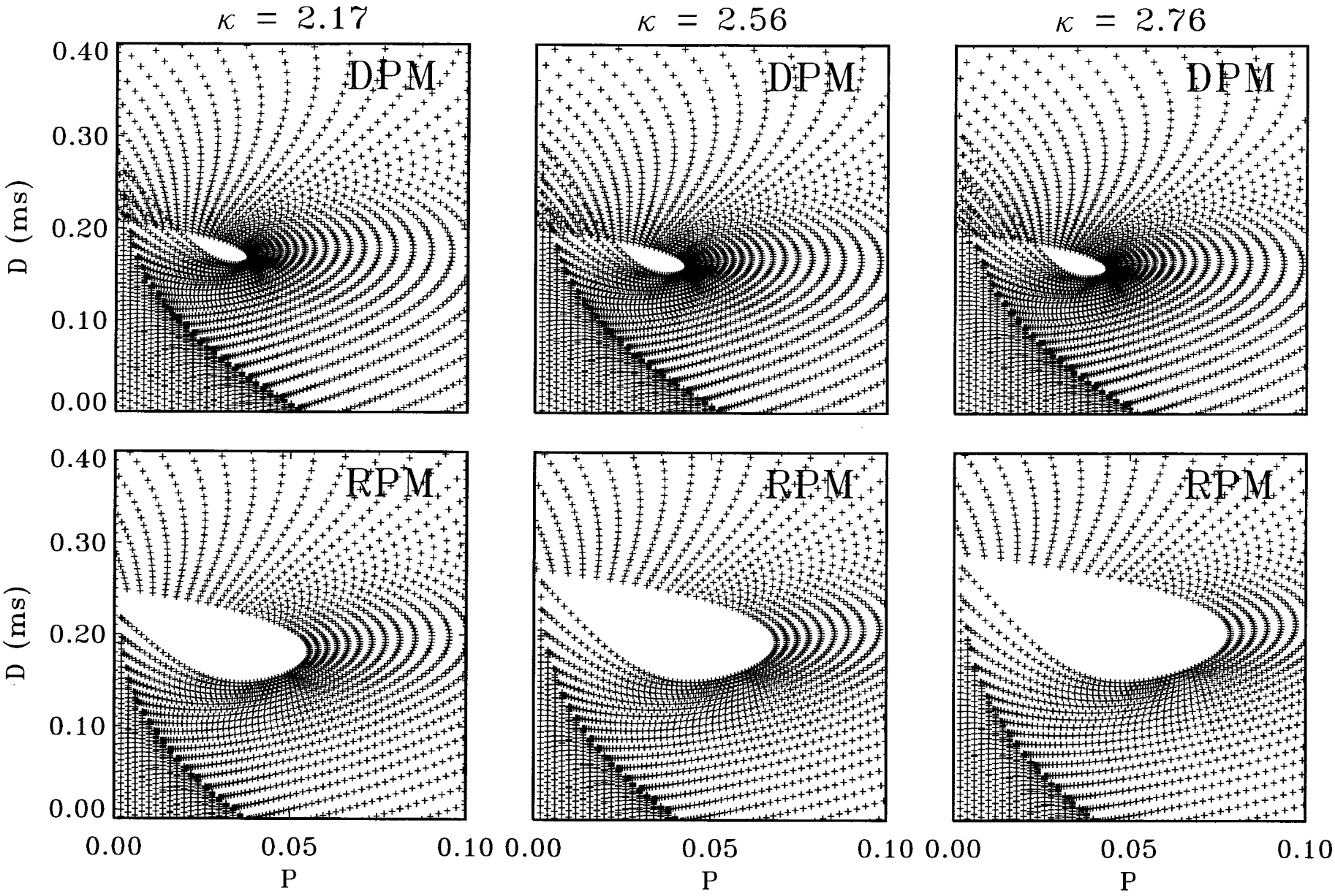

Fig.9.

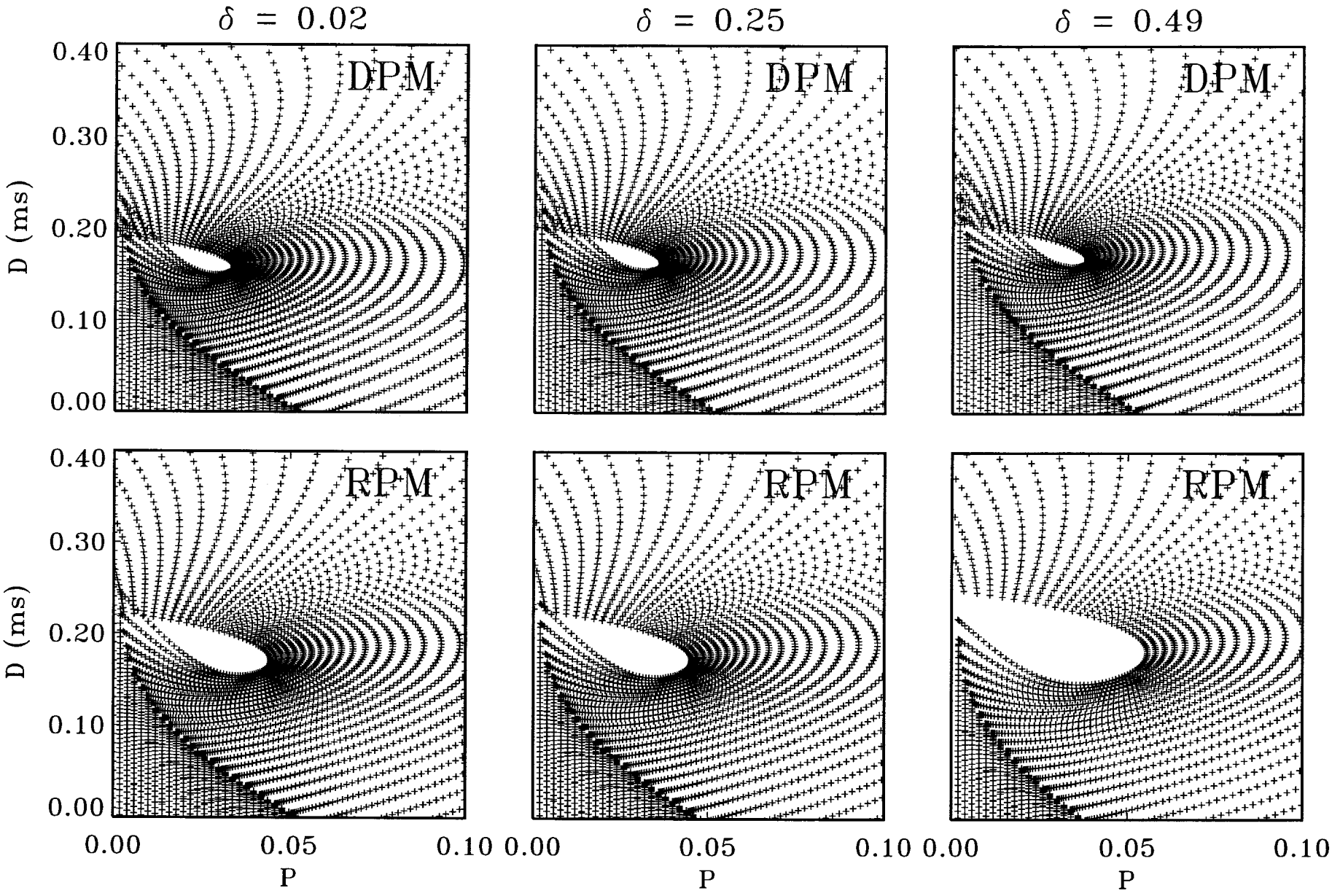

Fig.10.

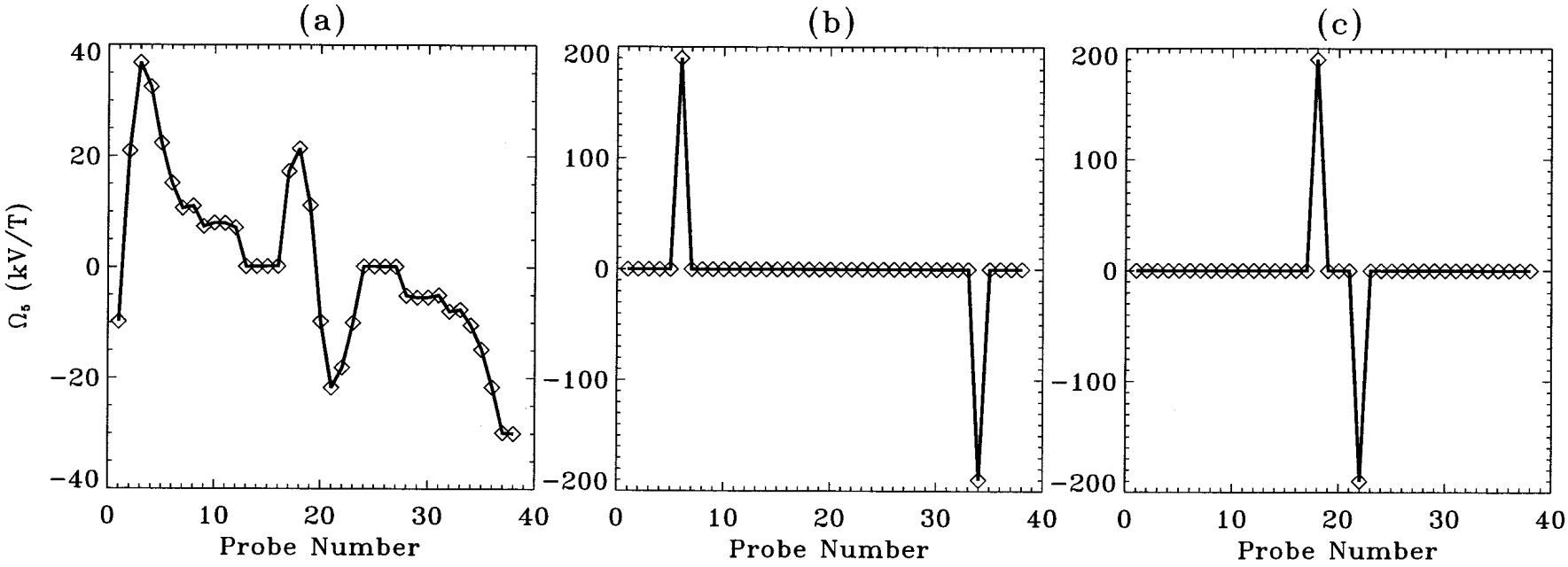

Fig.11.

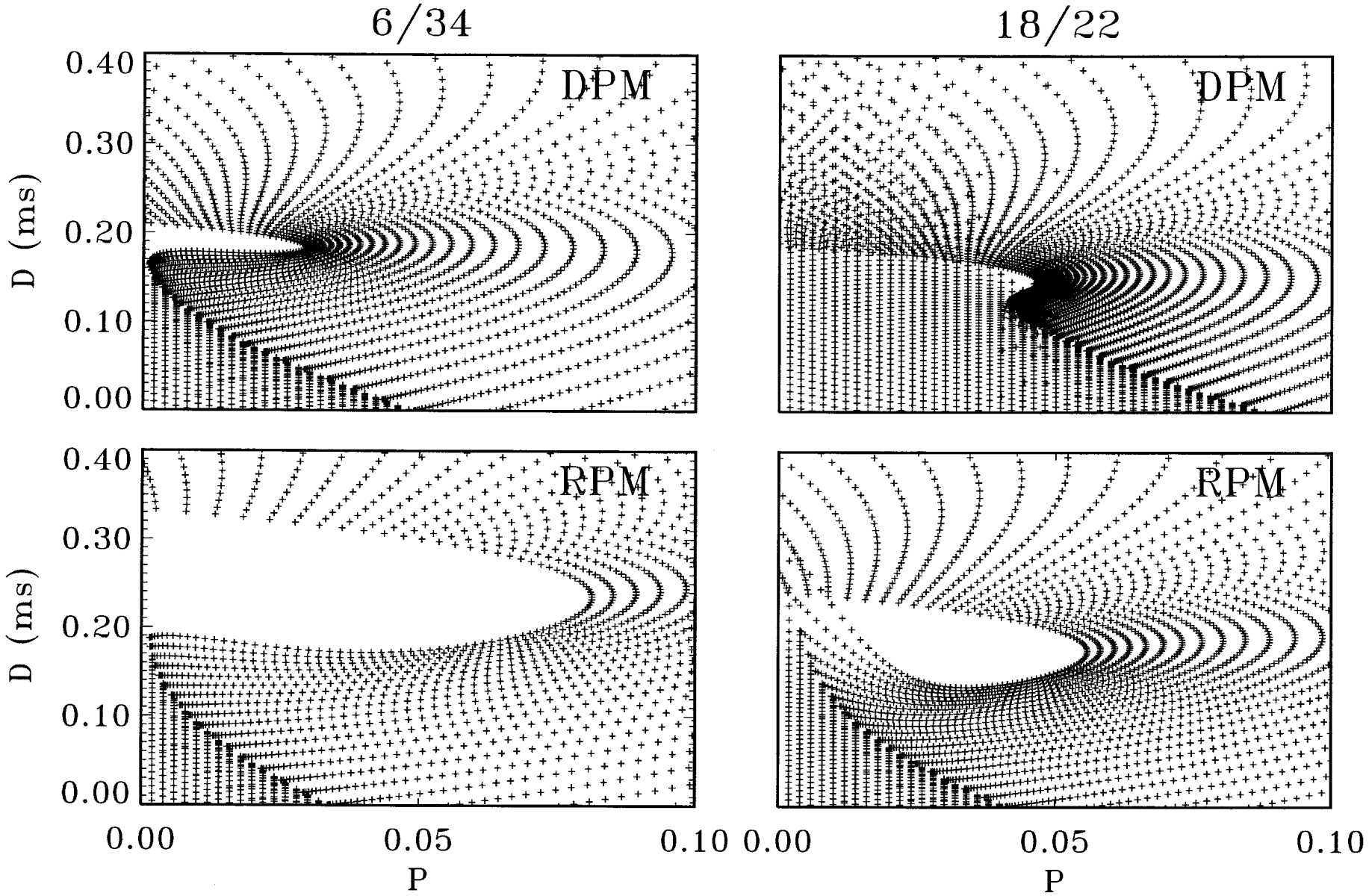
6/34
18/22
DPM
DPM
RPM
RPM
D (ms)
D (ms)
0.40
0.30
0.20
0.10
0.00
0.00
0.05
0.10
P

Fig.12.

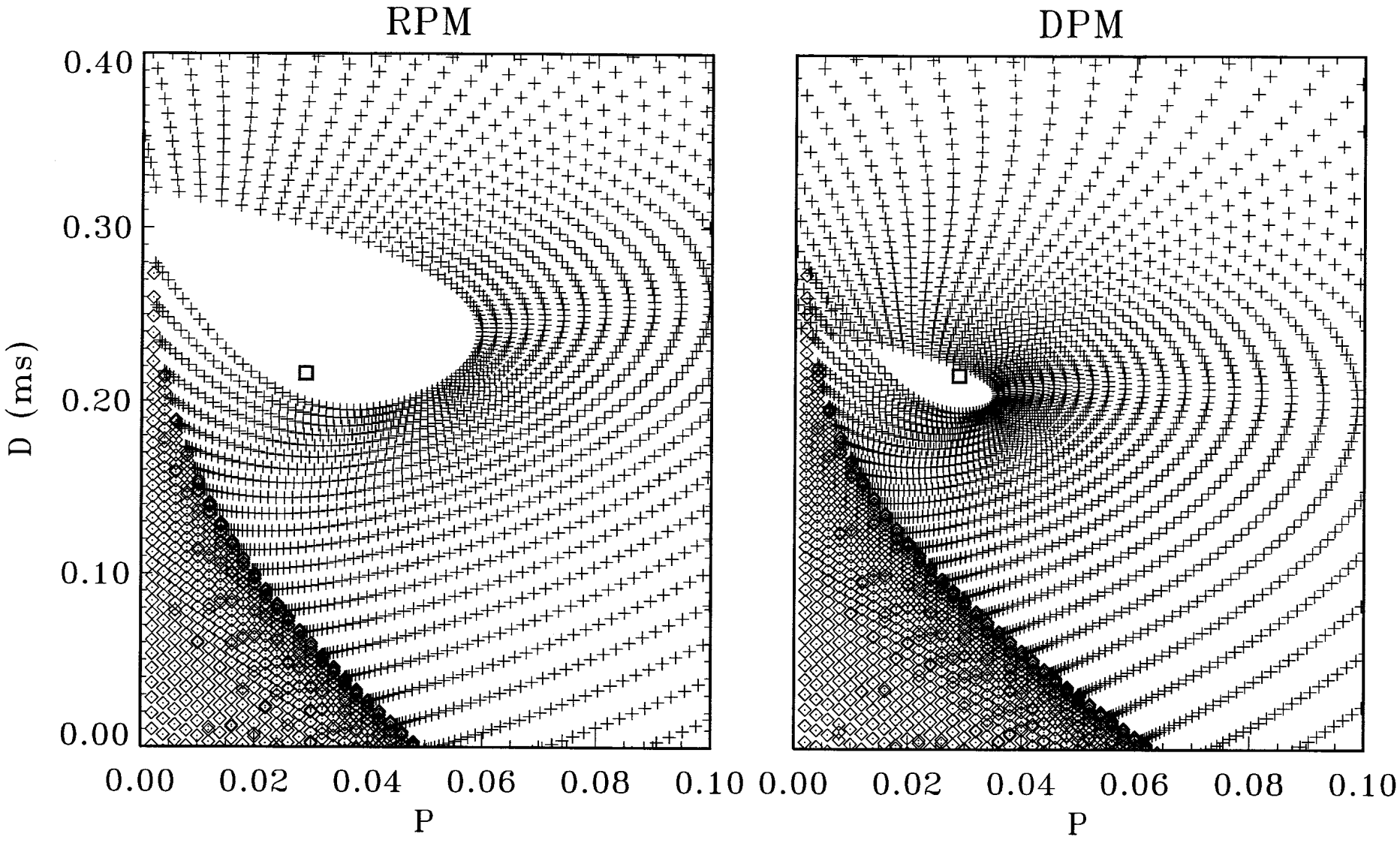

Fig.13.